Negative differential resistance in graphene nanoribbon superlattice field-effect transistors

Sheng Chang, Lei Zhao, Yawei Lv, Hao Wang, Qijun Huang, Jin He

Key Laboratory of Acoustic and Photonic Materials and Devices of Ministry of Education, School of Physics and Technology, Wuhan University, Wuhan 430072, People's Republic of China
E-mail: changsheng@whu.edu.cn

Published in Micro & Nano Letters; Received on 4th January 2015; Revised on 8th May 2015; Accepted on 8th May 2015

Different from researches in two-terminal nanoscale graphene structures, the negative differential resistance (NDR) phenomenon in graphene nanoribbon superlattice (GNSL) field-effect transistors (FETs) is studied in this reported work. Numerical analyses of two types of GNSL FETs with different gate voltages reveal that NDR occurs in some 'Z'-type GNSL FETs under some gate voltages, which develops NDR research compared with the traditional two-terminal nanoscale structures. Based on these results, two trends are observed: the $3m+2$ series GNSL FETs easily exhibit NDR, whereas it is more difficult to achieve this phenomenon with narrow FETs. This phenomenon is explained by the transmission coefficient as well as *ab-initio* calculations of the energy levels, where the entire channel of the FET is considered as a supercell. Through this analysis, the effect of gate control on energy-level localisation is uncovered, and a heterojunction-like explanation is proposed. This new explanation bridges the gap between a novel structure's physical analysis and the general semiconductor device concept, which can also provide inspiration for improving our understanding of novel nanostructure devices.

1. Introduction: As a candidate of the post-silicon era, graphene-based semiconductor devices have been intensively studied. Large-area graphene field-effect transistors (GFETs) [1] have been produced for high-frequency applications because of the high mobility of graphene. Uniform channel graphene nanoribbon field-effect transistors (GNR FETs) [2] have been designed for digital circuit applications based on their bandgap opening with a limited width. Following the idea of width modulation, graphene nanoribbon superlattices (GNSLs) have been fabricated recently. Similar to the development of a wide-bandgap M–S–M nanostructure by Hicks *et al.* [3], Liang *et al.* manufactured graphene nanomeshes with ribbon widths of <10 nm [4]. Sun *et al.* [5] fabricated sophisticated multifunctional superlattices by exchanging the sp3 C–H bonds in graphene with sp3 C–C bonds through functionalisation. Yang *et al.* [6] observed a two-dimensional superlattice of a trigonal moiré pattern by the plasma-assisted deposition method of the epitaxial growth of single-domain graphene on hexagonal boron nitride. Cranney *et al.* [7] intercalated small gold clusters between the top monolayer graphene and the buffer layer of epitaxial graphene to create superlattice resonators.

As a finite nanostructure, the carrier transport in a GNSL differs from that in large-scale graphene structures, a fact that has attracted much attention. For example, Motta *et al.* [8] studied the tunnel effect in armchair graphene nanoribbon junctions. Chen *et al.* [9] and Zhou *et al.* [10] investigated negative differential resistance (NDR) behaviour in doped crossed graphene nanoribbon junctions. Masum Habib *et al.* [11] achieved standing wave-type current–voltage (I–V) behaviour in a cross-structure consisting of two overlapping GNRs. Khasanvis *et al.* [12] used a similar structure to establish memory with silicon CMOS. Nguyen *et al.* [13] explored the NDR effect in graphene nanoribbon break junctions. Saha and Nikolic [14] explored the NDR effect in graphene-nanoribbon–carbon-nanotube crossbars. Masum Habib *et al.* [15] studied NDR in a bilayer GNR nanostructure. However, these studies only focused on the two-terminal characteristics of GNSLs. Work relating to three-terminal devices is rare. Alarcón *et al.* [16] studied the NDR in wide graphene field effect transistors. That NDR was caused by doping, but in GNSL structures the NDR can be caused by the channel geometric shape's inhomogeneity. They are different in both intrinsic carrier transport and terminal I–V characteristic. As far as we know, no work concerning the performance of nanoscale graphene FET structures with gate control has been reported. This situation prevents the application of graphene nanostructures in circuit design, as FETs are the most widely used devices in modern circuits.

Different from researches in traditional two-terminal graphene structures, the NDR of GNSL FETs is explored in this Letter. The I–V performances of different GNSL FETs are first calculated, demonstrating the relationship between NDR and the size and bias of the GNSL FET. A significant effect of the gate voltage (FETs' effect) is found, which was not demonstrated in the previous two-terminal nanoscale structures. Finally, the physics of this phenomenon is examined using a transmission coefficient method as well as a novel heterojunction-like explanation based on an in-depth analysis of the localised energy level.

2. NDR phenomenon in GNSL FETS: A GNSL is a nanoscale finite graphene pattern. By employing this pattern as a channel covered by an oxide and using a gate in contact with a source and a drain, one can obtain a GNSL FET. Considering that the symmetric cross pattern is the most widely researched GNSL, this pattern was selected as the channel for our FETs.

To observe the NDR phenomenon in GNSL FETs, FETs with different source/drain contacts ('H' and 'Z' types) and different sizes are explored under different terminal biases in this Section. Fig. 1 presents schematic diagrams of two typical GNSL FETs as representatives, where the number of carbon atoms in the cross region is marked as the serial number of the FET, such as H17 in Fig. 1*a* and Z17 in Fig. 1*b*. Since we focus on the effect of channel geometric shape modulation, an ideal interface between the dielectric layer and the channel is assumed in the calculation.

The output characteristics of the FETs under different gate biases are simulated by the non-equilibrium Green's function (NEGF) with a tight-binding Hamiltonian, in which the channel current is described by Landauer-Büttiker formalism. Typical results for the different GNSL FETs under different biases are shown in Fig. 2. These Figures indicate that the NDR behaviour in different

© The Institution of Engineering and Technology 2015

doi: 10.1049/mnl.2015.0131

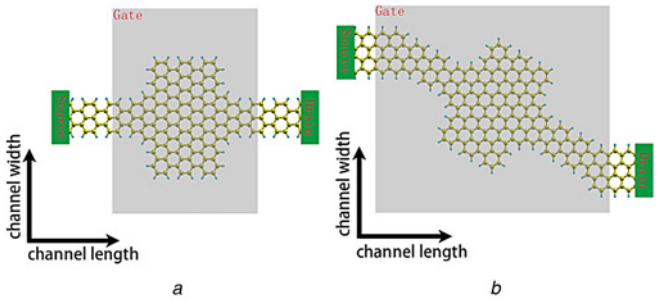


Figure 1 *Schematic representations of different GNSL FETs*
a 'H' style GNSL FETs (H17)
b 'Z' style GNSL FETs (Z17)

GNSL FETs is diverse. For the H15 and Z15 GNSL FETs, no obvious NDR can be observed under all given gate biases. For the Z17 GNSL FET, significant NDR arises under a specific bias but disappears under other biases, which cannot be explored in the traditional two-terminal structures. For the Z23 GNSL FET, NDR is observed for all gate biases studied, and its degree varies with gate voltage, which also shows the effect of gate bias. The transfer characteristic of Z17 FET is shown as Fig. 3. The fluctuation and crossover of the curves under different drain biases also verify the NDR phenomenon, such as the two sets of annotated curves correspond to the two NDR regions of Z17 FET with $V_{gs} = 0.2$ V.

To test our results over a wider range, further calculations were performed, in which none of the 'H' style GNSL FETs (H15, H17 and H19) exhibited significant NDR under all given gate biases. Therefore only the results of the 'Z' style GNSL FETs are listed in Table 1.

From Table 1, it is clear that when the size of the 'Z'-type GNSL FET is small, no negative conductance is observed. For large sizes, negative conductance occurs more frequently, except for Z19. However, using the absolute value of the negative conductance as the only criterion for NDR is not rigorous. In comparing FETs with different channel currents and similar negative conductance, the FET with the smaller channel current exhibits a more significant NDR phenomenon. Therefore the ratios of the valley and peak currents observed in the NDR region are listed in Table 2. As a criterion, when the ratio of the valley and peak currents is larger than 0.9, the case is stated to not exhibit significant NDR because that case is not only inconspicuous in the visual sense, but would also be unstable if applied in NDR-relative circuits. For example,

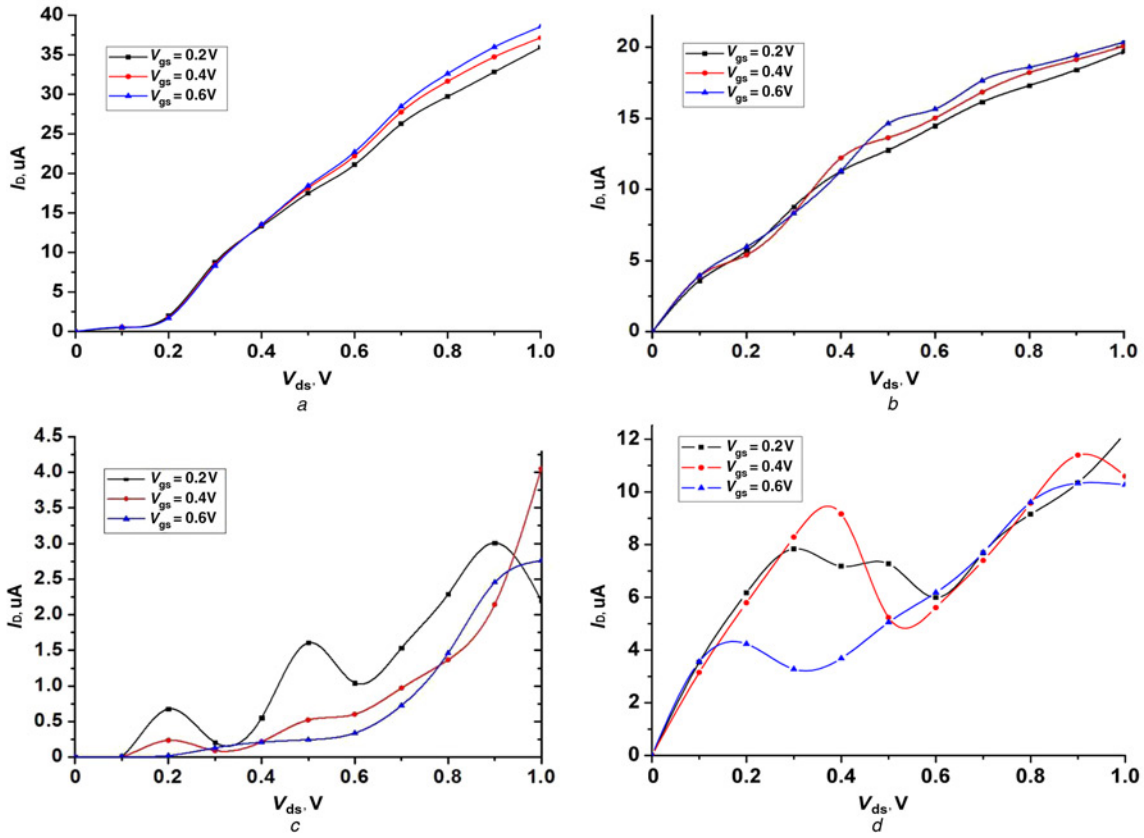


Figure 2 *NDR phenomenon in GNSL FETs*
a I–V curve of the H15 GNSL FET under different gate biases
b I–V curve of the Z15 GNSL FET under different gate biases
c I–V curve of the Z17 GNSL FET under different gate biases
d I–V curve of the Z23 GNSL FET under different gate biases

© The Institution of Engineering and Technology 2015

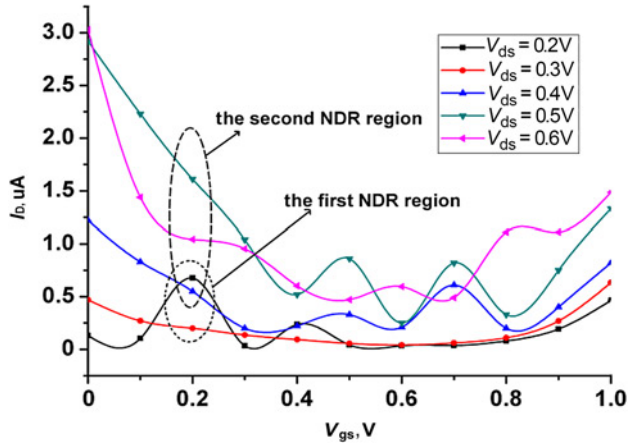


Figure 3 *I_d–V_{gs} characteristic for different gates at various V_{ds} in Z17 FET*

Z17 and Z21 with $V_{gs} = 0.4$ V have almost the same negative conductance, as shown in Table 1, but exhibit significantly different ratios. Therefore the former is judged to display significant NDR, whereas the latter is not.

Following these two standards, it is found that the NDR in Z-type GNSL FETs exhibits two trends. First, the $N = 3m + 2$ FETs easily exhibit NDR, e.g. Z23 and Z17 show significant NDR under almost gate bias. Secondly, it is more difficult to achieve NDR in the FETs with a narrow cross region; thus, Z11 displays no NDR, while Z21 and Z25 exhibit NDR in some cases.

3. Physics of NDR in GNSL FETS: From the above analysis, the behaviour of NDR in GNSL FETs has been determined. However, the mechanism behind this phenomenon remains unclear. A physical exploration of this phenomenon is discussed in this Section.

The transmission coefficient method has been widely used to describe the electrical characteristics of nanostructures. Fig. 4 provides an analysis from this aspect. In general, one case without NDR (the Z15 FET with $V_{gs} = 0.2$ V) and one case with NDR (the Z17 FET with $V_{gs} = 0.2$ V) are selected to demonstrate the results.

In Fig. 4, to make the results more visual, the bias windows with different V_{ds} are marked by some assisting vertical lines. For example, the bias window of $V_{ds} = 0.2$ V is shown by the black ±0.1 eV assisting lines. For the Z15 FET, when $V_{gs} = 0.2$ V, strong peaks can be observed for all four V_{ds} values in the bias windows, indicating that the FET has stable current transmission under different drain biases. Therefore in this case no NDR appears, as shown in Fig. 2*b*. In contrast, for the Z17 FET, when $V_{gs} = 0.2$ V, significant peaks can be observed only for the curves corresponding to $V_{ds} = 0.2$ and 0.5 V. For the curves corresponding to $V_{ds} = 0.3$ and 0.6 V, no peak appears in the bias window. In this case, as the drain voltage increases, the channel current increases and decreases and then increases again and decreases again. That means significant NDR, as shown in Fig. 2*c*.

Table 1 Negative conductance of the NDR region (μs)

V_{gs} (V)	Z9	Z11	Z13	Z15	Z17	Z19	Z21	Z23	Z25
0.2	N	N	N	N	−9.6	N	−5	−16	−6.5
0.4	N	N	N	N	−2.5	N	−2.4	−46	−6.7
0.6	N	N	N	N	N	N	−25	−11	N

N indicates no negative conductance.
If more than one NDR region exists, as in the case for the Z17 FET with $V_{gs} = 0.2$ V, the region with the largest negative conductance is selected.

Table 2 Ratio of valley and peak currents of the NDR region

V_{gs} (V)	Z17	Z21	Z23	Z25
0.2	0.31	0.77	0.83	0.92 (N)
0.4	0.39	0.94 (N)	0.57	0.88
0.6	N	0.53	0.78	N

N indicates that the case did not exhibit significant NDR.
If more than one NDR region exists, as in the case for the Z17 FET with $V_{gs} = 0.2$ V, the region with the largest negative conductance is selected.

To investigate this phenomenon in more detail, the energy-level structures of the GNSL FETs were explored using an *ab-initio* calculation based on density functional theory, which provides a novel explanation. In the numerical computation, since we focus on the influence of channel geometric shape modulation, only channel atoms are included and the source/drain contact effect is neglected.

The results for the H15, Z15 and Z17 GNSL FETs are presented in Fig. 5, where the energy levels of both FETs are localised following the spatial distribution of carbon atoms; the entire channel can be divided into three parts as labelled. For the H15 FET and the Z15 FET, the energy levels near the Fermi energy in all three parts are almost continuous; thus, the FETs act similar to a normal FET with a uniform channel, and no NDR occurs, as shown in Figs. 2*a* and *b*.

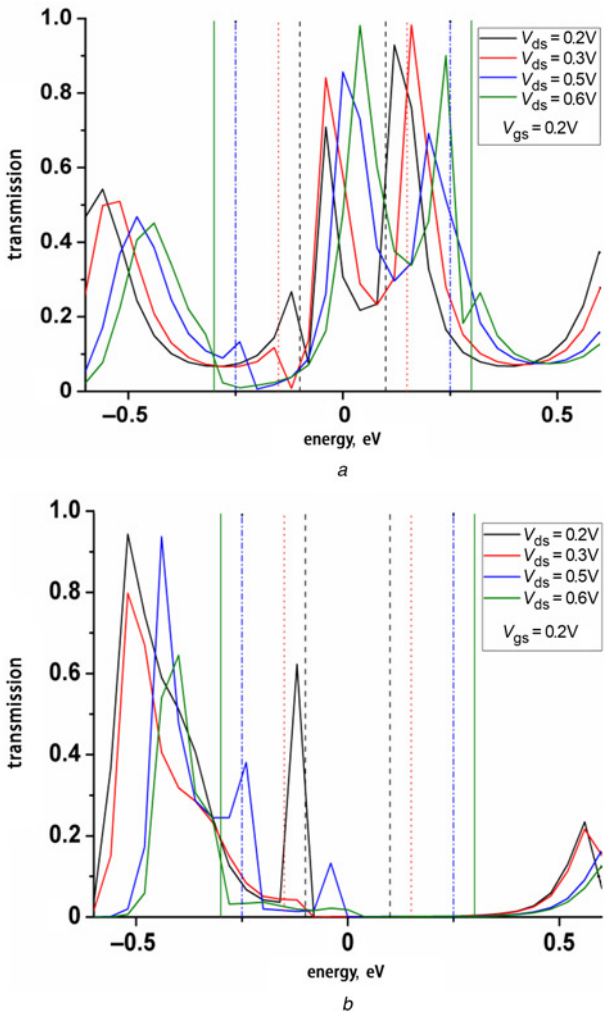


Figure 4 *Transmission coefficient analysis*
a Numerous peaks for the Z15 GNSL FET when $V_{gs} = 0.2$ V
b Sparse peaks for the Z17 GNSL FET when $V_{gs} = 0.2$ V

© The Institution of Engineering and Technology 2015

doi: 10.1049/mnl.2015.0131

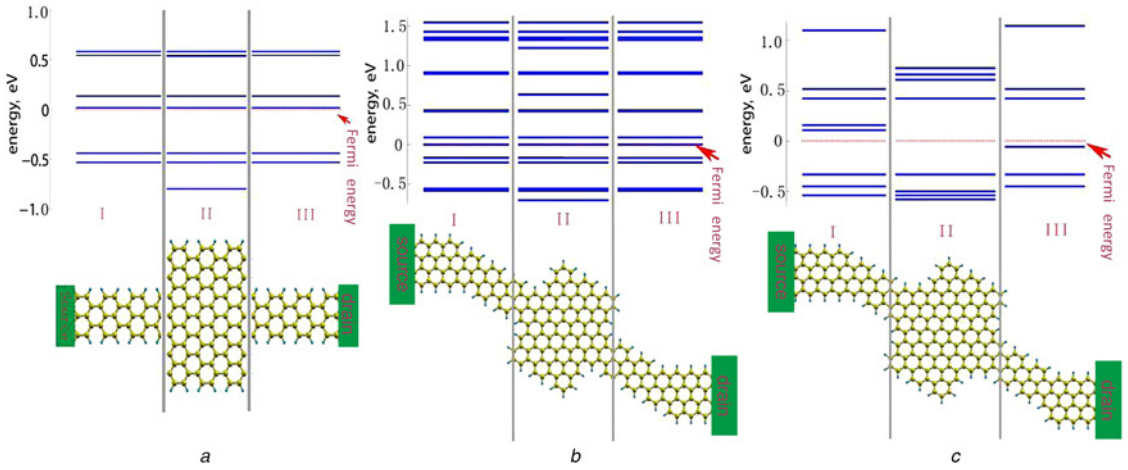


Figure 5 *Energy-level analysis*
a Localised energy levels of the H15 GNSL
b Localised energy levels of the Z15 GNSL
c Localised energy levels of the Z17 GNSL

However, these energy levels are discontinuous for the Z17 FET. In part I, the Fermi energy is near the lowest unoccupied level, displaying an N-type characteristic. In contrast, the behaviour in part II is similar to that of an I-type semiconductor, while the behaviour in part III is similar to that of a P-type semiconductor. Considering their different forbidden bandwidths (0.44, 0.75 and 0.5 eV, respectively), the Z17 FET can be envisioned as a heterojunction-like structure, in which NDR is possible. Specifically, when a small gate voltage is applied (0.2 V), the Fermi energy has a slight increase (the increase in part I is restrained because the lowest unoccupied energy level can supply abundant carriers). In this case, the physical picture changes only slightly; therefore NDR appears under the effect of V_{ds}, as shown in Fig. 2*c*. However, as V_{gs} increases (0.4 and 0.6 V), abundant electron carriers are generated in the channel. In all three parts of the channel, the lowest unoccupied energy levels are near the Fermi level. So all three parts tend to show a homogenous N-type characteristic. The above physical picture is destroyed, and the NDR disappears.

The above analysis uncovers the essence of NDR in GNSL FETs. The NDR phenomenon is the combinational result the of graphene nanoribbon superlattices' shape, terminal voltage (drain voltage) and gate voltage, while the last factor has not been uncovered in previous works. This explanation bridges the gap between the novel structure's physical analysis and the general semiconductor device concept, which can also provide inspiration for other nanostructure devices.

4. Conclusion: In this Letter, a novel FET with a graphene nanoribbon superlattice channel is constructed, and the NDR phenomenon observed in the device is discussed. The results demonstrate that $N = 3m + 2$ FETs easily exhibit NDR, whereas it is more difficult to achieve this phenomenon in narrow FETs. A novel heterojunction-like explanation based on energy calculations of the GNSL FETs is proposed, which not only illustrates the NDR in GNSL FETs but is also helpful in deepening our understanding of novel nanoscale devices.

5. Acknowledgments: This work was supported by the National Natural Science Foundation of China (grant nos. 61204096 and 61404094), the Fundamental Research Fund for the Central Universities, Wuhan University (grant no. 2042014kf0238), the China Postdoctoral Science Foundation (grant no. 2012T50688) and the Science Foundation of Jiangsu Province, China (grant no. BK20141218).

6 References

[1] Liao L., Lin Y.C., Bao M., *ET AL.*: 'High-speed graphene transistors with a self-aligned nanowire gate', *Nature*, 2010, **467**, pp. 305–308
[2] Liang G., Neophytou N., Nikonov D.E., Lundstrom L.S.: 'Performance projections for ballistic graphene nanoribbon field-effect transistors', *IEEE Trans. Electron Dev.*, 2007, **54**, pp. 677–682
[3] Hicks J., Tejeda A., Taleb-Ibrahimi A., *ET AL.*: 'A wide-bandgap metal-semiconductor-metal nanostructure made entirely from graphene', *Nat. Phys.*, 2013, **9**, pp. 49–54
[4] Liang X., Jung Y.S., Wu S., *ET AL.*: 'Formation of bandgap and subbands in graphene nanomeshes with sub-10 nm ribbon width fabricated via nanoimprint lithography', *Nano Lett.*, 2010, **10**, pp. 2454–2460
[5] Sun Z.Z., Pint C.L., Marcano D.C., *ET AL.*: 'Towards hybrid superlattices in grapheme', *Nat. Commun.*, 2011, **2**, pp. 1–5
[6] Yang W., Chen G.R., Shi Z.W., Liu C.C.: 'Epitaxial growth of single-domain graphene on hexagonal boron nitride', *Nat. Mater.*, 2013, **12**, pp. 792–797
[7] Cranney M., Vonau F., Pillai P.B., *ET AL.*: 'Superlattice of resonators on monolayer graphene created by intercalated gold nanoclusters', *Europhys. Lett.*, 2010, **91**, p. 66004
[8] Motta C., Sanchez-Portal D., Trioni M.I.: 'Transport properties of armchair graphene nanoribbon junctions between graphene electrodes', *Phys. Chem. Chem. Phys.*, 2012, **14**, pp. 10683–10689
[9] Chen L.N., Ma S.S., Ouyang F.P., Wu X.Z., Xiao J., Xu H.: 'Negative differential resistance behaviour in N-doped crossed graphene nanoribbons', *Chin. Phys. B*, 2010, **19**, p. 97301
[10] Zhou B., Zeng A., Zhou G.: 'Electronic transport for pristine and doped crossed graphene nanoribbon junctions with zigzag interfaces', *Phys. Lett. A*, 2012, **376**, pp. 1710–1713
[11] Masum Habib K.M., Zahid F., Lake R.K.: 'Multi-state current switching by voltage controlled coupling of crossed graphene nanoribbons', *J. Appl. Phys.*, 2013, **114**, p. 153710
[12] Khasanvis S., Rahman M., Moritz C.A.: 'Heterogeneous graphene-CMOS ternary content addressable memory', *J. Parallel Distrib. Comput.*, 2014, **74**, pp. 2497–2503
[13] Nguyen P.D., Nguyen T.C., Hossain F.M., Huynh D.H., Evans R., Skafidas E.: 'Negative differential resistance effect in planar graphene nanoribbon break junctions', *Nanoscale*, 2015, **7**, pp. 289–293
[14] Saha K.K., Nikolic B.K.: 'Negative differential resistance in graphene-nanoribbon-carbon-nanotube crossbars: a first-principles multiterminal quantum transport study', *J. Comput. Electron.*, 2013, **12**, pp. 542–552
[15] Masum Habib K.M., Ahsan S., Lake R.K.: 'Computational study of negative differential resistance in graphene bilayer nanostructures', *Proc. SPIE*, 2011, **8101**, p. 81010Q
[16] Alarcón A., Nguyen V.H., Berrada S., *ET AL.*: 'Pseudosaturation and negative differential conductance in graphene field-effect transistors', *IEEE Trans. Electron Dev.*, 2013, **60**, pp. 985–991

© The Institution of Engineering and Technology 2015